Journal of Ceramic Processing Research. Vol. 9, No. 1, pp. 25~29 (2008)

J O U R N A L O F
Ceramic Processing Research

Growth and photoluminescience properties for $CuInSe_2$ epilayers made by a hot wall epitaxy method

Seukjin Yun[a], Kwangjoon Hong[b,*] and Hyeonyoung Park[c]

[a]*Department of Chemistry Education, Chosun University, Gwangju 501-759, Korea*
[b]*Department of Physics, Chosun University, Gwangju 501-759, Korea*
[c]*Department of Biology, Chosun University, Gwangju 501-759, Korea*

Copper indium diselenide ($CuInSe_2$, CIS) layers were grown on GaAs(100) substrates using a hot wall epitaxy (HWE) method. The optimum temperatures of the substrate and the source for the growth turned out to be 410 and 620 °C, respectively. The CIS layers were epitaxially grown along the <112> direction and kept the initial mole fraction during the layer growth. Based on an absorption measurement, the band-gap variation of CIS was well interpreted by Varshni's equation. However, the energy difference, 180 meV, of the band gap between liquid helium and room temperatures was a very large value, unlike that reported for CIS. Also, from the low-temperature photoluminescence measurement, the acceptor impurities in the CIS layers were confirmed to be native defects of V_{Cu} and/or Se_{int}, which were deeply located at 73.8 meV above the edge of the valence band.

Key words: $CuInSe_2$ film, optimum growth condition, band gap energy, acceptor impurity, photoluminescience.

Introduction

Copper indium diselenide ($CuInSe_2$, CIS), which crystallizes to the chalcopyrite structure, has received considerable attention in recent years because of its application in photovoltaic devices [1-3]. Moreover, it is one of the most environmental-friendly materials for Cd-free buffer layers because of its high absorbance in the UV visible range [4]. Currently, CIS-based solar cells have been reported to achieve a high conversion efficiency of 18.8% [5]. Thus, CIS for solar cells is: (1) capable of high efficiency in spite of a thin thickness of 1-2 μm, (2) a cheap material in comparison to crystalline Si sharing about 90% of the Si solar-cell market, (3) and a material having better electro-optical stability over a long time. However, the electro-optical properties of CIS strongly depend on native defects due to deviation of the stoichiometry. Therefore, reduction of the stoichiometry deviation during crystal growth is required. As such, CIS layers have been grown by many different techniques such as metalorganic chemical vapor deposition (MOCVD), metalorganic vapor phase epitaxy (MOVPE), and molecular beam epitaxy (MBE), chemical bath deposition (CBD), electrodeposition (ED), RF sputtering, chemical spray pyrolysis (CSP), and electron beam evaporation [6-13]. In fact, hot wall epitaxy (HWE), which has been used to grow a high-purity ZnSe epitaxial layer at low temperatures [14], is one of the better methods for CIS growth. Thus, HWE has been especially designed to grow epilayers under the condition of near thermodynamic equilibrium [15, 16]. But, CIS growth by HWE method has rarely been reported before now.

In this paper, we proceed to grow high-quality CIS epitaxial layers using HWE. The optimum conditions of the grown CIS layers was investigated by means of the photoluminescence (PL) technique. Also, the composition ratio of each element of the grown epitaxial layers was checked by an energy dispersive X-ray spectrometer (EDS). From these results, we discuss the structural and optical properties of the grown CIS epitaxial layers.

Experimental

Prior to the layer growth, CIS polycrystalline was formed as follows. The starting materials were 6 N purity shot-types of Cu, In, and Se. A quartz tube was sequentially cleaned with trichlorethylene, acetone, methanol, and deionized water. After the materials were weighed in the mole fraction of each element, they were sealed in a quartz tube to maintain a vacuum atmosphere. The sealed ampoule was placed in the synthesis furnace and was continually rotated at a rate of 1 revolution per minute. In order to avoid explosion of the ampoule, the temperature of the ampoule was increased gradually to 1050 °C, which was then maintained for 48 h. To grow the CIS epitaxial layers, the ingot of CIS polycrystalline was used as a HWE

*Corresponding author:
Tel : +82-62-230-6637
Fax: +82-62-234-4326
E-mail: kjhong@chosun.ac.kr

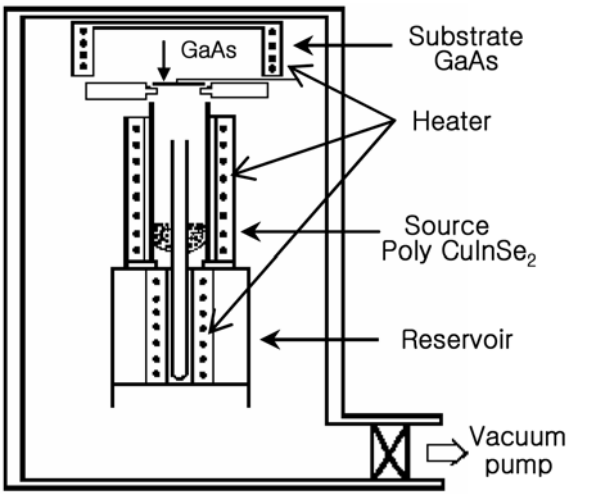

Fig. 1. Schematic diagram of the HWE apparatus used for the CIS growth.

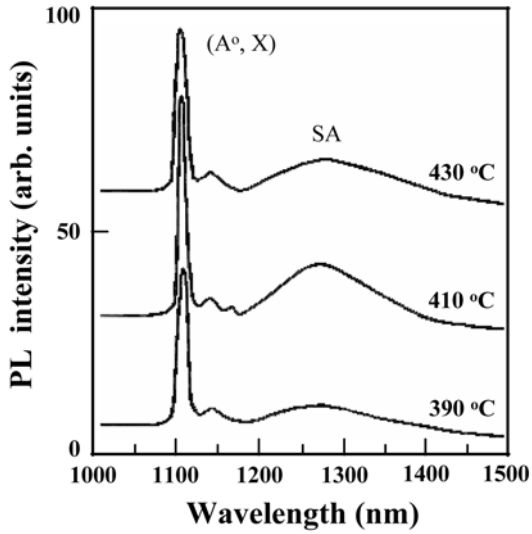

Fig. 2. PL spectra according to the variation of the substrate temperature.

source. The CIS layers were grown on semi-insulating GaAs (100) by the HWE method. Figure 1 shows HWE apparatus used for the CIS growth. The GaAs substrate was cleaned ultrasonically for 1 minute in successive baths of trichloroethylene, acetone, methanol and 2-propanol and etched for 1 minute in a solution of H_2SO_4:H_2O_2:H_2O (5:1:1). The substrate was degreased in organic solvents, and rinsed with deionized water. After the substrate was dried off, the substrate was immediately loaded onto the substrate holder in Fig. 1 and was annealed at 580 ºC for 20 minute to remove the residual oxide on the surface of the substrate. After the growth was finished, the grown CIS layers were subjected to PL measurements to find the optimum growth conditions. The PL experiment was performed at 10 K in a low temperature cryostat during the excitement of the He-Cd laser. The thickness of the CIS was measured by an α-step profilometer (Tenco, α-step 200). Also, X-ray diffraction (XRD) and energy dispersive X-ray spectrometer (EDS) experiments were used to confirm the orientation and the composition of the CIS layers, respectively. An optical absorption experiment to measure the band-gap energy was performed with a UV-VIS-NIR spectrophotometer for a range of 1040 to 1240 nm with the temperature varying from 10 to 293 K.

Results and Discussion

Epitaxial layer growth and structural characterization

After the heat treatment of the substrate surface, the CIS layers were grown at one of the substrate temperatures of 390, 410 and 430 ºC, while the source temperature was fixed at 620 ºC. At this time, the crystal quality of the grown CIS layers was evaluated by measuring the PL spectra at 10 K. The exciton emissions were used to predict the crystal-quality criterion of the grown layer because the exciton could only be observed in a less defective crystal at a low temperature. Here, a neutral acceptor bound exciton of (Å, X) and self-activated (SA) emissions were used for the optimum growth conditions. The grown layers are considered to have good crystal quality when the measured PL spectra shows that the intensity of (Å, X) tends to increase and the intensity of the SA is inclined to decrease. Thus, the full width half maximum (FWHM) value of the PL spectrum was considered together. Figure 2 shows the PL spectra of the CIS layers grown with a variation of the substrate temperature when the source temperature was fixed at 620 ºC. From the PL spectra, the grown CIS layers showed the shape of p-type crystallites. As shown in Fig. 2, the (Å, X) peak in the layer, which was grown while the substrate temperature was kept at 410 ºC, had the highest intensity of all the samples. The narrowest FWHM, which indicates high crystal quality, was observed in the CIS layer grown at 410 ºC as well. By contrast, the intensities of the SA peaks are comparatively low at all growth temperatures. With a source temperature of 620 ºC obtained by experimental repetition, the most suitable substrate temperature for the growth turned out to be 410 ºC. Thus, the grown CIS layers were obtained to a thickness of 2.7 μm and a growth rate of 0.9 μm/h. Figure 3 shows the surface morphology of a scanning electron microscope image (SEM) on a CIS layer grown at 410 ºC. As shown in Fig. 3, the morphology revealed a very smooth surface, and it consisted of nano-size crystallites having a size of 40-70 nm. Figure 4 presents the XRD curves of the CIS layers grown with a variation of the substrate temperature. As shown in Fig. 4, the optimized condition was confirmed to be the CIS layer grown at 410 ºC like the PL result. Thus, the patterns obtained correspond to the diffraction peaks of the CIS (112) and GaAs (004). The intensity of the CIS (112) peak located at two theta of 26.623º is

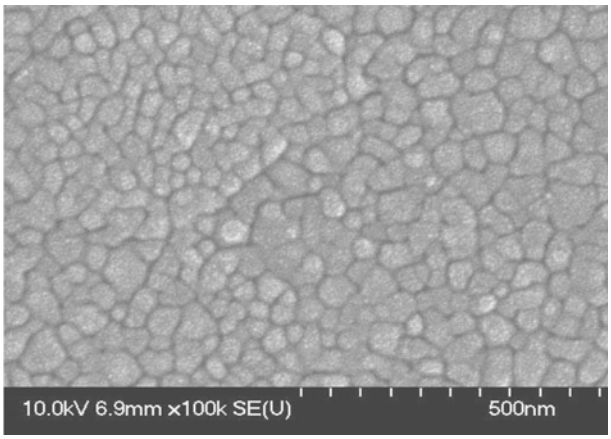

Fig. 3. Surface morphology of a SEM image on CIS layer.

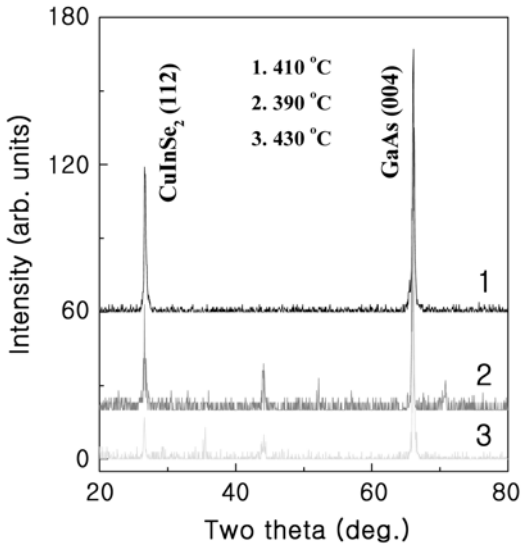

Fig. 4. XRD curves of the CIS layers grown with the variation of the substrate temperature.

very sharp and dominant. This means that the orientation of the layer grown on the GaAs (100) substrate is converted to the (112) plane. This phenomenon was also observed in the CdTe epilayer grown on a GaAs (100). Faurie et al. [17] reported that the orientation of the CdTe epilayer was related to the pre-annealing process used to remove the residual oxide on the surface of the substrate. They concluded that the growth of the CdTe (100) or (111) planes on the GaAs (100) was possible by controlling the different annealing temperatures and times of the substrate. On the other hand, the observation of only one peak of the CIS (112) indicates that the CIS layer was grown epitaxially along the <112> direction onto the GaAs (100) substrate. This orientation is suggested to be beneficial for a CIS layer to be fabricated for solar energy conversion [18]. Also, one theta value of the FWHM on (112) peak is 0.15°. Introducing the Scherrer formula [19] in order to evaluate the mean crystallite size of the film:

Table 1. Composition ratios of each element on the synthesized polycrystalline and the CIS layer analyzed by the EDS measurement. (units: atomic %)

Elements	Synthesized polycrystalline		Layer	
	Before synthesis	After synthesis	Before growth	After growth
Cu	18.896	19.121	19.121	19.084
In	34.144	34.243	34.243	34.256
Se	46.960	46.636	46.636	46.660

$$D=0.94\lambda/(B\cos\theta), \quad (1)$$

where λ, θ, and B are the X-ray wavelength (0.15405 nm), the Bragg diffraction angle, and the FWHM value on (112) peak in radians, respectively. The mean crystallite size obtained from Eq. (1) was estimated to be about 55 nm. Therefore, the crystalline size evaluated by XRD was consistent with the SEM result.

Table 1 presents the compositions of each element during the growth process of the CIS layer, analyzed by EDS measurements. As shown in Table 1, the compositions of the initial mole fractions were continuously maintained during the layer growth. Consequently, it is suggested that the grown CIS layer was formed stoichiometrically bond.

Optical properties

Figure 5 shows the optical absorption spectra obtained in the temperature range of 10 K to 293 K. To identify the band-gap energy for the CIS layer, we carefully examined the relation between the optical absorption coefficient (α) and the incident photon energy (hν) from the optical absorption measurements in Fig. 5. The relation for a direct band gap between hn and α is given by:

$$(\alpha h\nu)^2 \sim (h\nu - E_g). \quad (2)$$

According to Eq. (2), $(\alpha h\nu)^2$ linearly depends upon the photon energy. From the plots of $(\alpha h\nu)^2$ versus photon energy for different temperatures, the band gaps are

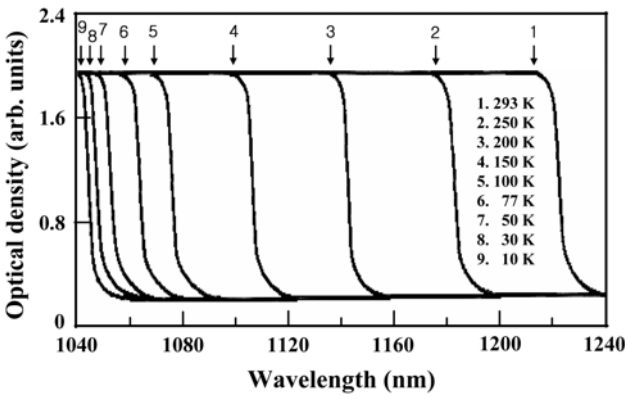

Fig. 5. Optical absorption spectra according to the variation of the measurment temperature.

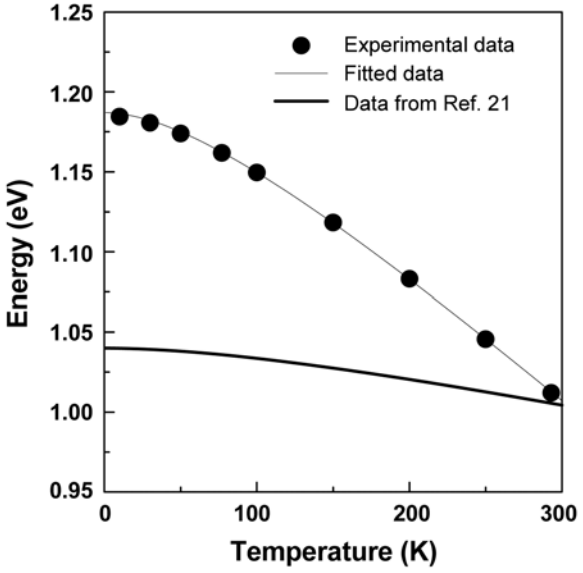

Fig. 6. Band-gap variation of the CIS layer as a function of temperature.

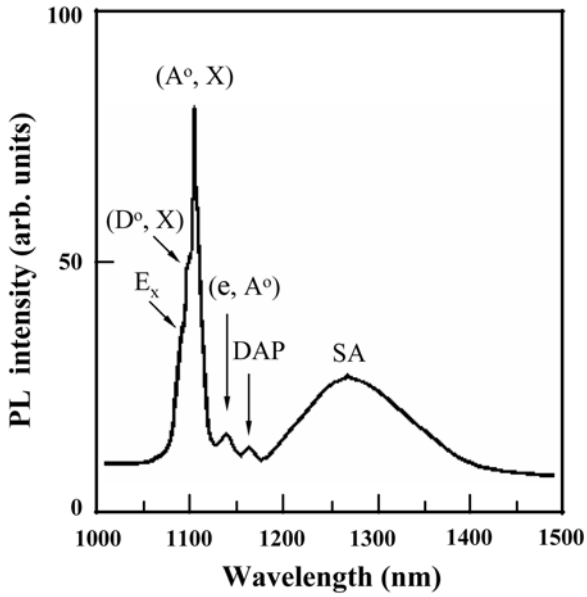

Fig. 7. PL spectrum of the CIS layer measured at 10 K.

determined by extrapolating the linear portions of the respective curves to $(\alpha h\nu)^2 = 0$. Figure 6 displays the band-gap variation of the CIS layer as a function of temperature. The temperature dependence of the band-gap energy in our experiment is well fitted numerically by the following formula [20-22]:

$$E_g(T)=E_g(0)-aT^2/(T+b), \quad (3)$$

where a is a constant and b is approximately the Debye temperature. Also, $E_g(0)$ is the band-gap energy at 0 K, which is estimated to be 1.187 eV. When a and b are taken to be 8.57×10^{-4} eV/K and 129 K, respectively, the curve plotted by Eq. (3) closely fits the experimental values. But, as shown in Fig. 6, the energy difference of the band gap between liquid helium and room temperatures is about 180 meV and this value is very large in comparison with 33 meV of a CIS grown by MBE [23]. This is caused by the absence of a considerable concentration of defects and lattice strain at the low temperatures. Therefore, it suggests that the increase of E_g is due to the activation of high photon-energy transitions as a result of the high quality crystallinity in the layer. Indeed, it means that the crystalline quality of the grown CIS layer is better than that of CIS grown by MBE or other methods.

Figure 7 shows a typical PL spectrum of the CIS layer measured at 10 K. The two peaks on the shoulder appear at 1098.7 (1.1284 eV) and 1100 nm (1.1247 eV) toward the shorter-wavelength region. These peaks are associated with the free exciton (E_x) and the neutral donor bound exciton (D^o, X) caused by the recombination from free exciton to neutral donor, respectively. The binding energy, E_x^b, of E_x is given by:

$$E_x^b=E_g(10)-E_x, \quad (4)$$

where $E_g(10)$ is the band-gap energy at 10 K. The value of $E_g(10)$ was calculated to be 1.1863 eV using Eq. (3) and the E_x^b is obtained to be 57.9 meV. This value is larger than the reported one [24] and is close to the E_x^b of ZnO having 60 meV. On the other hand, the strong peak of (Å, X) appears at 1104.5 nm (1.1225 eV) as shown in Fig. 7. This belongs to the typical p-type configuration of the PL spectrum observed in the CIS layer. This bound exciton has been known to be related to the recombination from free exciton to neutral acceptor. The origin of (Å, X) emission can be ascribed to the deep acceptor level originatins from the copper vacancy (V_{Cu}) due to a stoichiometric deviation. Also, the binding energy (E_A) of the acceptor impurity is obtained by:

$$E(A^o, X)=E_x-0.08E_A, \quad (5)$$

where E_A is calculated to be 73.8 meV. The optical transitions of E_A may be associated with a deep level of sulfur interstitial (S_{int}) or V_{Cu} point defects. There is a possibility of the acceptor state of the V_{Cu} and/or Se_{int}, which is deeply located at 73.8 meV upper the edge of the valence band. The weak peak of 1137.6 nm (1.0899 eV) appeared at the shoulder of the (Å, X) peak toward the longer-wavelength region. This peak is associated with the free to bound emission (e, Å) due to the recombination of a free electron to the neutral acceptor. In addition, donor-acceptor pairs (DAP) emission at 1161.2 nm (1.0677 eV) was observed. The DAP emission occurred due to the interaction between the donor and the acceptor states in the band-gap energy. The relatively low and broad peak caused by the SA emission was observed at 1282.1 nm (0.9670 eV) in the longer-wavelength region. This emission relates closely to the native defects formed in the CIS layer.

Conclusions

The CIS layers were successfully grown on GaAs(100) substrates by the HWE method. The optimum temperatures for the growth turned out to be 410 °C for substrate and 620 °C for source. Under optimized condition, the CIS layer was confirmed to the epitaxially grown layer along the <112> direction onto the GaAs (100) substrate. Thus, from the EDS measurement, the grown CIS layers were consistent with a stoichiometric composition maintaining the initial mole fraction during the layer growth. The band-gap variation of CIS attracted by the absorption measurement was well fitted by $E_g(T)=E_g(0)-aT^2/(T+b)$. The a and b were taken to be 8.57×10^{-4} eV/K and 129 K, respectively. But, the energy difference of the band gap between liquid helium and room temperatures was about 180 meV. This value is nearly larger three times than that reported of the conventional CIS. This fact indicates that the crystalline quality of the grown CIS layer is better than that of CIS grown by MBE or other methods. Also, from the low-temperature PL measurements, the E_x^b of the E_x and the E_A of the acceptor impurity on the CIS layers turned out to be 57.9 and 73.8 meV, respectively. Therefore, the acceptor impurity in the CIS layer is suggested to be native defects of the V_{Cu} and/or Se_{int}, which are deeply located at 73.8 meV upper the edge of the valence band.

Acknowledgment

This study was supported by research funds from Chosun University, 2007.

References

1. J.L. Shay, and J.H. Wernick, Ternary Chalcopyrite Semiconductors: Growth, Electronic Properties, and Applications, (Pergamon, Oxford, 1975), Ch. 2.
2. Chang-Dae Kim, Gye-Choon Park, Moon-Seog Jin and Duck-Tae Kim, J. Korean Phys. Soc. 48 (2006) 951-956.
3. K.H. Lam, J. Close, and W. Durisch, Solar Energy 77 (2004) 121-124.
4. M. Yamaguchi, J. Appl. Phys. 78 (1995) 1476-1480.
5. M.A. Contreas, B. Egaas, K. Ramanathan, J. Hiltner, A. Swartzlander, F. Hasoon, and R. Noufi, Prog. Photovolt. Res. Appl. 7 (1997) 311-315.
6. M.C. Artaud, F. Ouchen, L. Martin, and S. Duchemin, Thin Solid Film 324 (1998) 115-119.
7. N. Rega, S. Siebentritt, I. Beckers, J. Beckmann, J. Albert, and M. Lux-Steiner, J. Cryst. Growth 248 (2003) 169-173.
8. S. Niki, P.J. Fons, Y. Lacroix, K. Iwata, A. Yamada, H. Oyanagi, M. Uchino, Y. Suzuki, R. Suzuki, S. Ishibashi, T. Ohdaira, N. Sakai, and H. Yokokawa, J. Cryst. Growth 201/202 (1999) 1061-1065.
9. K. Bindu, C.S. Kartha, K.P. Vijayakumar, T. Abe, and Y. Kashiwaba, Sol. Energy Mater. Sol. Cells 79 (2003) 67-71.
10. C.J. Huang, T.H. Meen, M.Y. Lai, and W.R. Chen, Sol. Energy Mater. Sol. Cells 82 (2004) 553-557.
11. T. Watanabe, M. Matsui, and K. Mori, Sol. Energy Mater. Sol. Cells 35 (1994) 239-243.
12. T.T. John, K.C. Wilson, P.M.R. Kumar, C.S. Kartha, K.P. Vijayakumar, Y. Kashiwaba, T. Abe, and Y. Yasuhiro, Phys. Stat. Sol. (a) 202 (2005) 79-83.
13. S.I. Casteneda and F. Rueda, Thin Solid Films 361 (2000) 145-149.
14. T.S. Jeong, P.Y. Yu, K.J. Hong, T.S. Kim, C.J. Youn, Y.D. Choi, K.S. Lee, B.O., and M.Y. Yoon, J. Cryst. Growth 249 (2003) 9-14.
15. A. Lopez-Otero, Thin Solid Films 49 (1987) 3-8.
16. Seoungnam Baek and Kwangjoon Hong, J. Korean Phys. Soc. 48 (2006) 1520-1524.
17. J.P. Faurie, C. Hsu, S. Sivananthan, and X. Chu, Surf. Sci. 168 (1986) 473-478.
18. M.D. Kannan, R. Balasundaraprabhu, S. Jayakumar, and P. Ramanathaswamy, Sol. Energy Mater. Sol. Cells 81 (2004) 379-283.
19. B.D. Cullity, Elements of X-Ray Diffractions (Addition-Wesley, Reading, MA, 1978), pp. 102-111.
20. Y.P. Varshni, Physica 34 (1967) 149-153.
21. Sukjin Yun and Kwangjoon Hong, J. Korean Phys. Soc. 45 (2004) S661-665.
22. Moon-Seog Jin, J. Korean Phys. Soc. 48 (2006) 681-685.
23. K. Yoshino, H. Yokoyama, K. Maeda, T. Ikari, A. Fukuyama, P. J. Fons, A. Yamada, and S. Niki, J. Appl. Phys. 86 (1999) 4354-4357.
24. S. Chichibu, T. Mizutani, K. Murakami, T. Shioda, T. Kurafuji, H. Nakanashi, S. Niki, P. J. Fons, and A. Yamada, J. Appl. Phys. 83 (1998) 3678-3681.